New phosphorescent platinum(II) complexes with tetradentate C*N^N*C ligands: liquid crystallinity and polarized emission

Shilin Zhang,[a] Kaijun Luo,*[a] Hao Geng,[a] Hailiang Ni,[a] Haifeng Wang[a] and Quan Li*[a]

College of Chemistry and Materials Science, Sichuan Normal University, 5 Jingan Road, Chengdu 610068 China

Electronic Supporting Information (ESI)

Table S1 Crystal data and structure refinement for **Pt-L[12]**.

	Pt-L[12]
Empirical formula	$C_{46}H_{62}N_2O_4Pt$
Formula weight	902.06
Temperature/K	293.1(2)
Crystal system	triclinic
Space group	P-1
a/Å	8.0093(2)
b/Å	9.9381(4)
c/Å	27.1665(9)
α/°	84.786(3)
β/°	86.532(3)
γ/°	70.962(3)
Volume/Å^3	2034.55(13)
Z	2
ρ_{calc}g/cm^3	1.472
μ/mm^{-1}	3.493
F(000)	924
Crystal size/mm^3	0.7 × 0.4 × 0.05

Radiation	MoKα (λ = 0.71073)
2θ range for data collection/°	6.702 to 50.7
Index ranges	$-9 \leq h \leq 9$, $-11 \leq k \leq 11$, $-32 \leq l \leq 32$
Reflections collected	25032
Independent reflections	7441 [R_{int} = 0.0509, R_{sigma} = 0.0472]
Data/restraints/parameters	7441/0/480
Goodness-of-fit on F^2	1.056
Final R indexes [I>=2σ (I)]	R_1 = 0.0302, wR_2 = 0.0697
Final R indexes [all data]	R_1 = 0.0344, wR_2 = 0.0726
Largest diff. peak/hole / e $Å^{-3}$	0.73/-1.96

Table S2. Solvatochromic Data for **Pt-L[16]**.

Solvent	Absorption bands (nm)	Emission (nm)
Toluene	440, 508	624
THF	430, 494	622
DMF	416, 474	619
Benzonitrile	415, 472	618

Table S3 Selected calculated excitation energies (ΔE), oscillator strengths (f), main orbital components, and Assignment for **Pt-L[16]**, **Pt-L[12]** and **Pt-L[6]** in dichloromethane.

	λ_{exc} (calc.)/nm	ΔE/eV	f	Transition (Percentage Contribution)	Assignment
Pt-L[16]	542.5	2.29	0.0518	H-0->L+0(+98%)	MLCT/ILCT
	436.7	2.84	0.0443	H-1->L+0(+70%), H-3->L+0(+27%)	MLCT/ILCT
	423.6	2.93	0.0513	H-3->L+0(+53%), H-1->L+0(+25%), H-2->L+0(+22%)	MLCT/ILCT
	401.4	3.09	0.0137	H-2->L+0(+75%), H-3->L+0(+19%)	MLCT/ILCT
	354.7	3.50	0.0173	H-0->L+1(+89%), H-4->L+0(+7%)	MLCT/ILCT
	351.5	3.53	0.0801	H-4->L+0(+88%), H-0->L+1(+6%)	MLCT/ILCT
Pt-L[12]	549.5	2.26	0.0527	H-0->L+0(+98%)	MLCT/ILCT
	438.0	2.83	0.0276	H-1->L+0(+53%), H-3->L+0(+41%), H-2->L+0(5%)	MLCT/ILCT
	426.9	2.90	0.0624	H-1->L+0(+42%), H-3->L+0(31%), H-2->L+0(+26%)	MLCT/ILCT
	403.5	3.07	0.0231	H-2->L+0(+66%), H-3->L+0(+27%)	MLCT/ILCT
	360.0	3.44	0.0148	H-0->L+1(+94%)	MLCT/ILCT
	354.1	3.50	0.0123	H-0->L+2(+84%), H-4->L+0(+10%)	MLCT/ILCT
	352.0	3.52	0.0897	H-4->L+0(+83%), H-0->L+2(11%)	MLCT/ILCT
Pt-L[6]	536.4	2.31	0.0549	H-0->L+0(+98%)	MLCT/ILCT
	439.3	2.82	0.0207	H-1->L+0(+54%), H-3->L+0(+45%)	MLCT/ILCT
	423.9	2.93	0.0845	H-3->L+0(+36%), H-2->L+0(+34%), H-1->L+0(+29%)	MLCT/ILCT
	414.9	2.99	0.0110	H-2->L+0(+63%), H-3->L+0(+18%), H-1->L+0(+16%)	MLCT/ILCT
	355.2	3.49	0.0653	H-4->L+0(+65%), H-0->L+1(+27%)	MLCT/ILCT
	353.1	3.51	0.0133	H-0->L+1(+67%), H-4->L+0(+29%)	MLCT/ILCT

Table S4 Selected bond lengths (Å) and angles (deg) for **Pt-L^{16}** from X-ray and TD-DFT calculations.

	X-ray	TD-DFT calculation
Pt(01)-C(008)	2.005(4)	2.016
Pt(01)-C(00A)	1.999(4)	2.015
Pt(01)-N(003)	2.053(3)	2.103
Pt(01)-N(002)	2.058(3)	2.103
C(00A)-Pt(01)-C(008)	97.95(15)	98.96
N(003)-Pt(01)-N(002)	79.59(12)	78.63
C(00A)-Pt(01)- N(002)	91.60(13)	92.18
C(008)-Pt(01)- N(003)	92.33(14)	92.07

Table S5 Thermal behavior for the new platinum(II) complexes.

Complex	Phase transition[a]/℃			Enthalpy changes (Δ H/kJ mol^{-1})
Pt-L^{16}	Cr_1	64	Cr_2	6.5
	Cr_2	130	Iso	10.1
	Iso	116	S_m	11.5
	S_m	57	Cr	8.1
Pt-L^{12}	Cr_1	58	Cr_2	5.4
	Cr_2	93	Cr_3	1.1
	Cr_3	120	Cr_4	3.0
	Cr_4	144	Iso	12.7
	Iso	127	S_m	10.2
	S_m	108	Cr_4	3.5
	Cr_4	52	Cr_3	15.0
	Cr_3	25	Cr_1	
Pt-L^{6}	Cr_1	35	Cr_2	3.0
	Cr_2	190	Iso	19.7
	Iso	155	Cr_2	18.9
	Cr_2	153	Cr_1	2.0

[a] Transition temperatures and enthalpy values are taken from the second DSC cycle starting from the crystal (10℃min^{-1}). Cr_1, Cr_2, Cr_3, Cr_4 = crystalline phase, Iso =isotropic liquid phase, S_m = smectic phase.

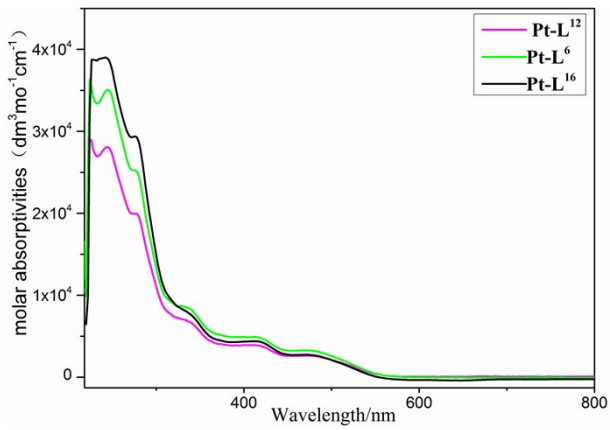

Fig. S1 UV-visible absorption of three platinum complexes in CH_2Cl_2 (≈1.2×10^{-5} mol dm^{-3}) at 298 K (λ_{ex} = 412 nm).

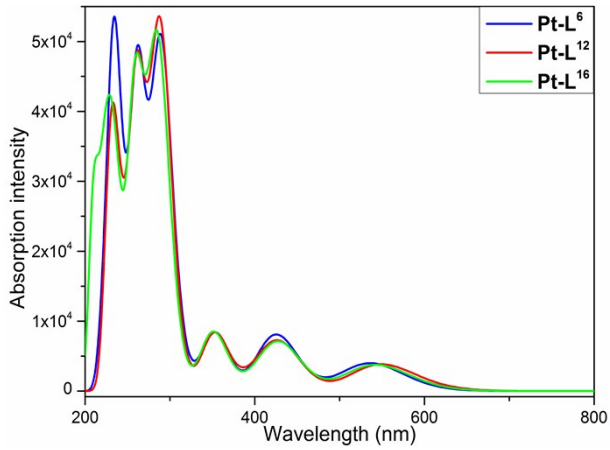

Fig. S2 Absorption spectra of **Pt-L^{12}** calculated at their optimized S_0 geometry in CH_2Cl_2 solution by TD-DFT.

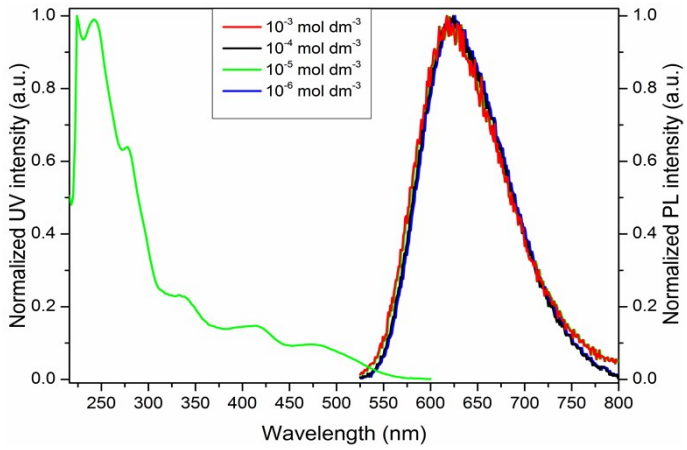

Fig. S3 Emission spectra of **Pt-L^{16}** in different concentrations in CH_2Cl_2 at 298 K (λ_{ex} = 412 nm).

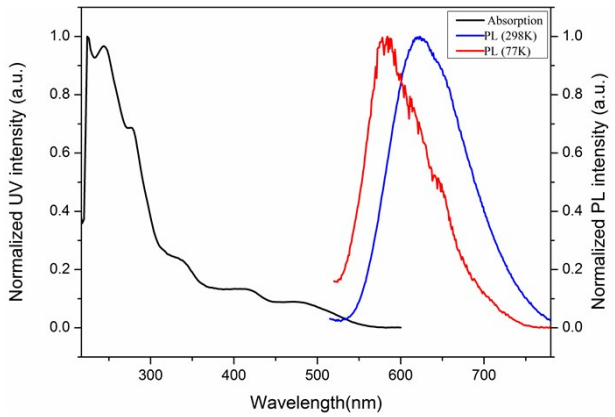

(a)

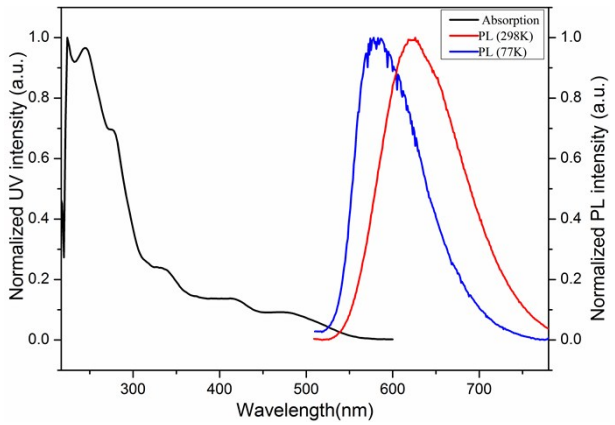

(b)

Fig. S4 UV-visible absorption and emission spectra of **Pt-L[12]** (a) and **Pt-L[6]** (b) in CH_2Cl_2 (≈1.2×10^{-5} mol dm^{-3}) at 298 K and 77 K (λ_{ex} = 412 nm)

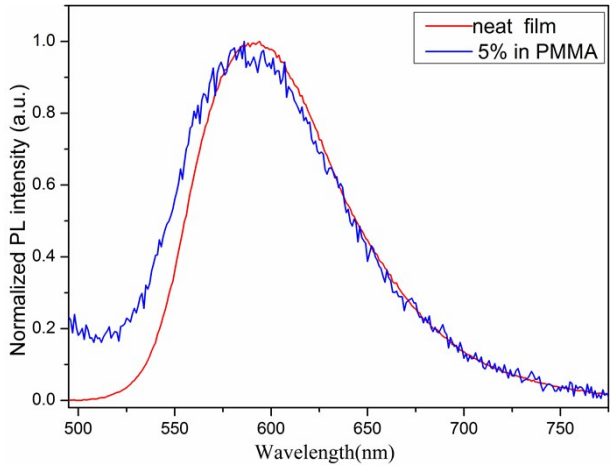

(a)

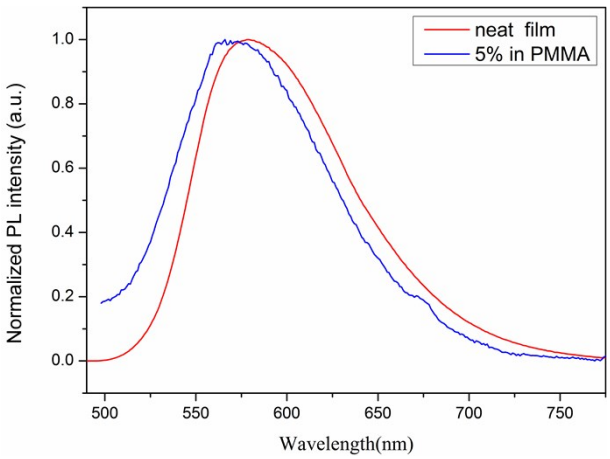

(b)

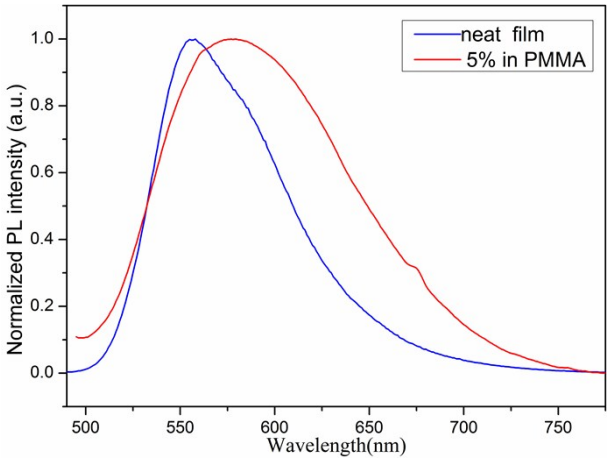

(c)

Fig. S5 Emission spectra of **Pt-L[16]** (a), **Pt-L[12]** (b), and **Pt-L[6]** (c) in neat film and a dopped PMMA film at 298 K (λ_{ex} = 412 nm).

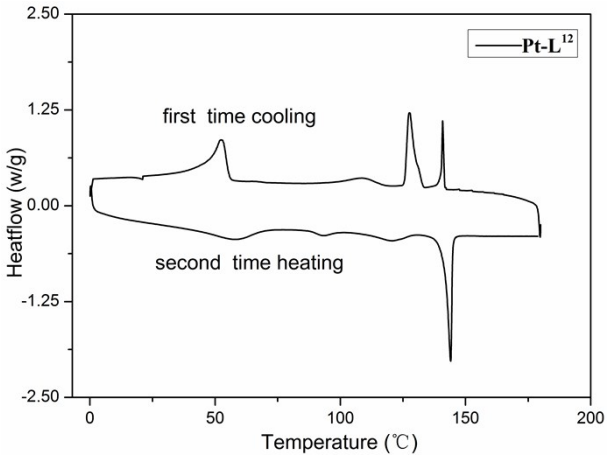

Fig. S6 DSC heating and cooling curves of **Pt-L[12]**.

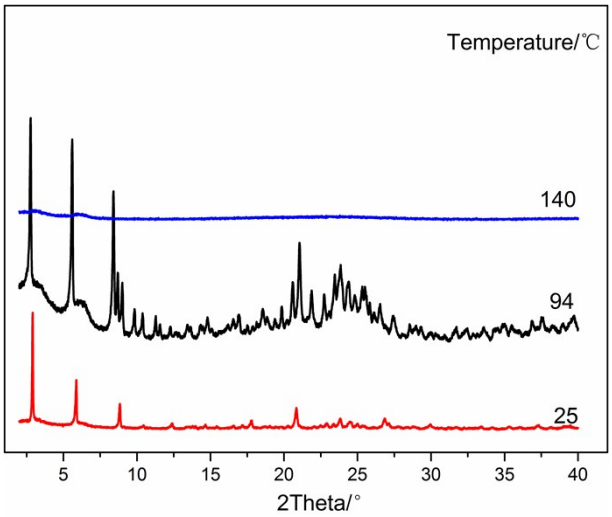

Fig. S7 Variable-temperature XRD patterns of **Pt-L**[16] on heating process.

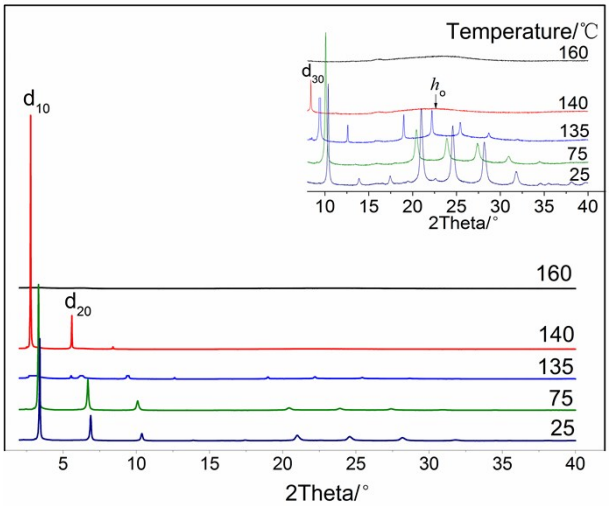

(a)

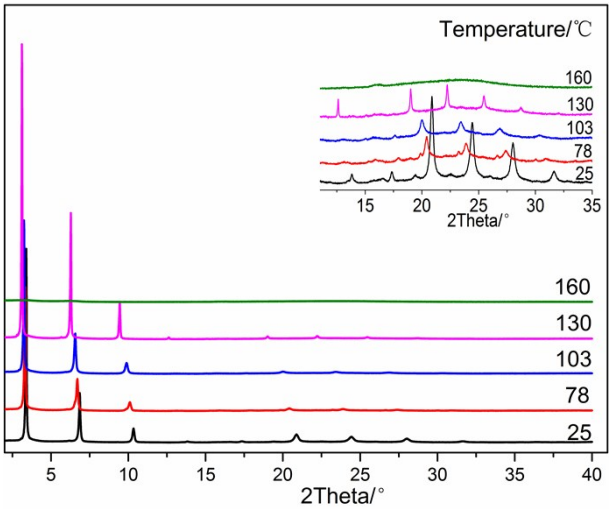

(b)

Fig. S8 Variable-temperature XRD patterns of **Pt-L**[12] on cooling process (a) and heating process (b). Inset shows

the magnified XRD patterns at high-angle regions.

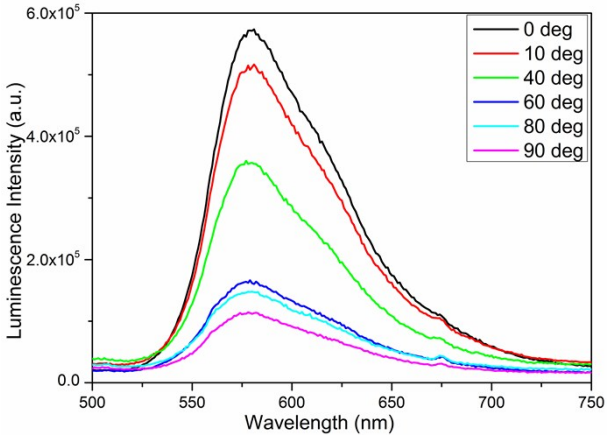

Fig. S9 PL spectra of the aligned **Pt-L^{16}** at different degrees of polarization.

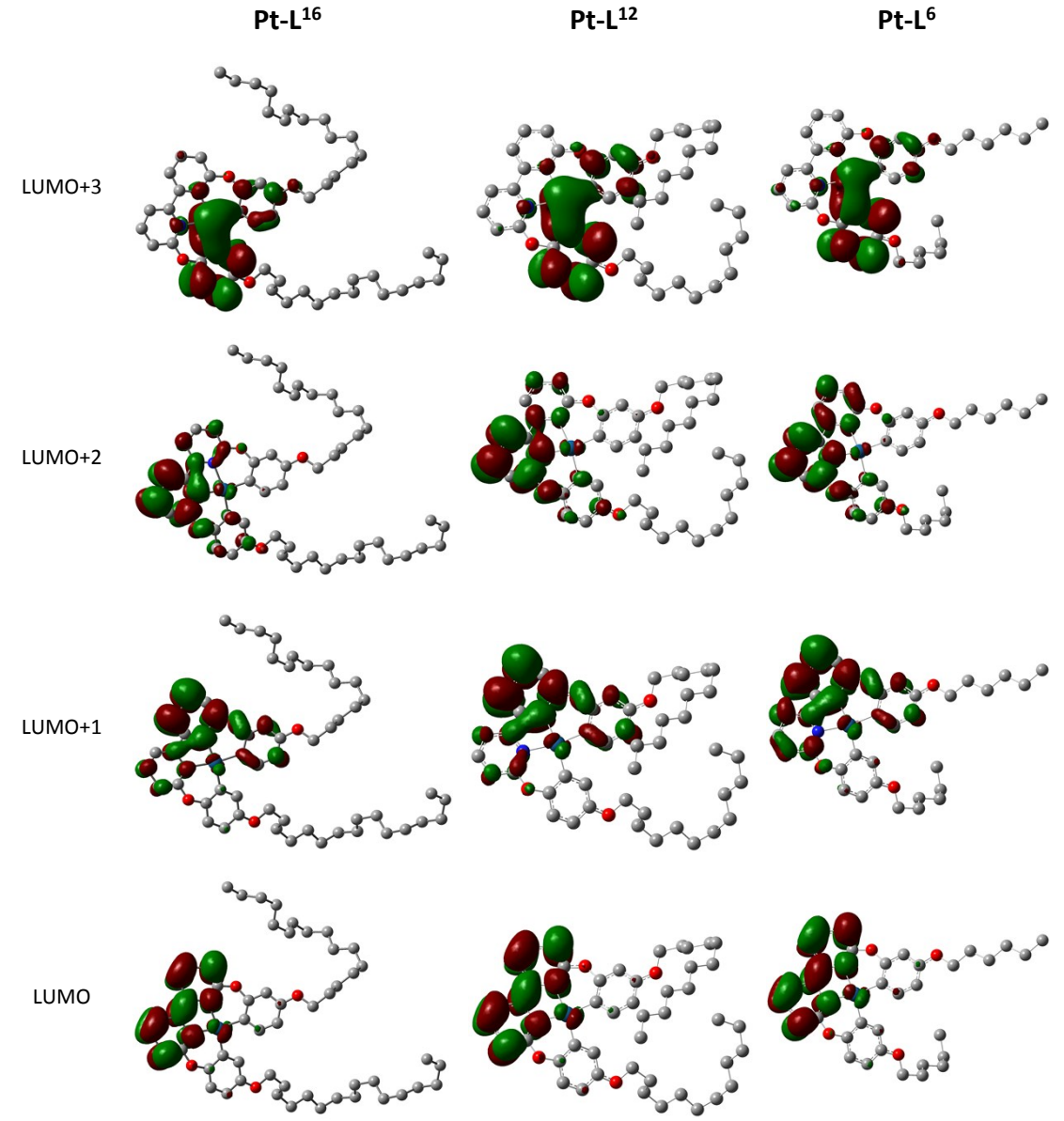

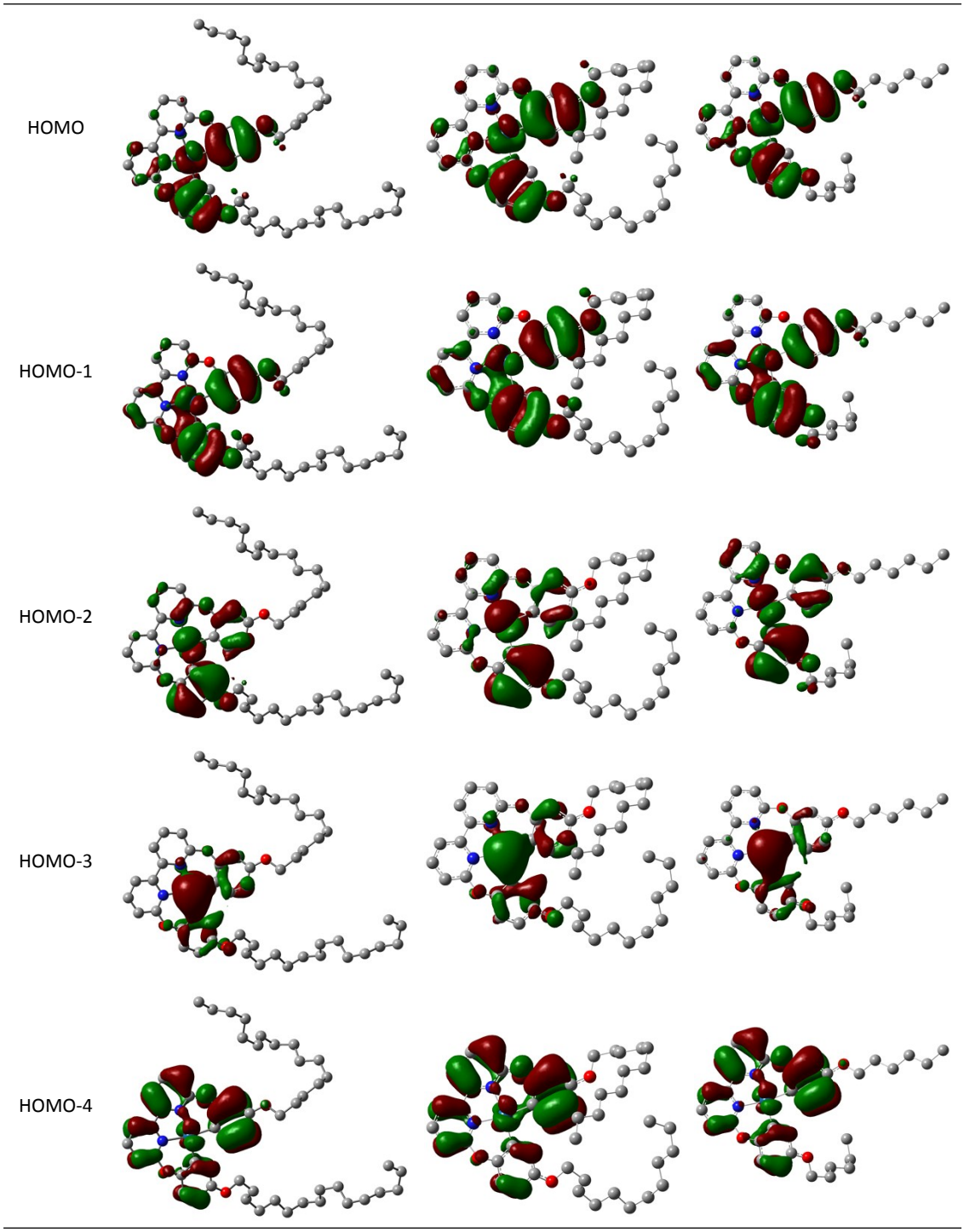

Fig. S10 Representative frontier orbitals for **Pt-L^{16}**, **Pt-L^{12}** and **Pt-L^{6}**.

^{1}H NMR plot of **Pt-L^6**.

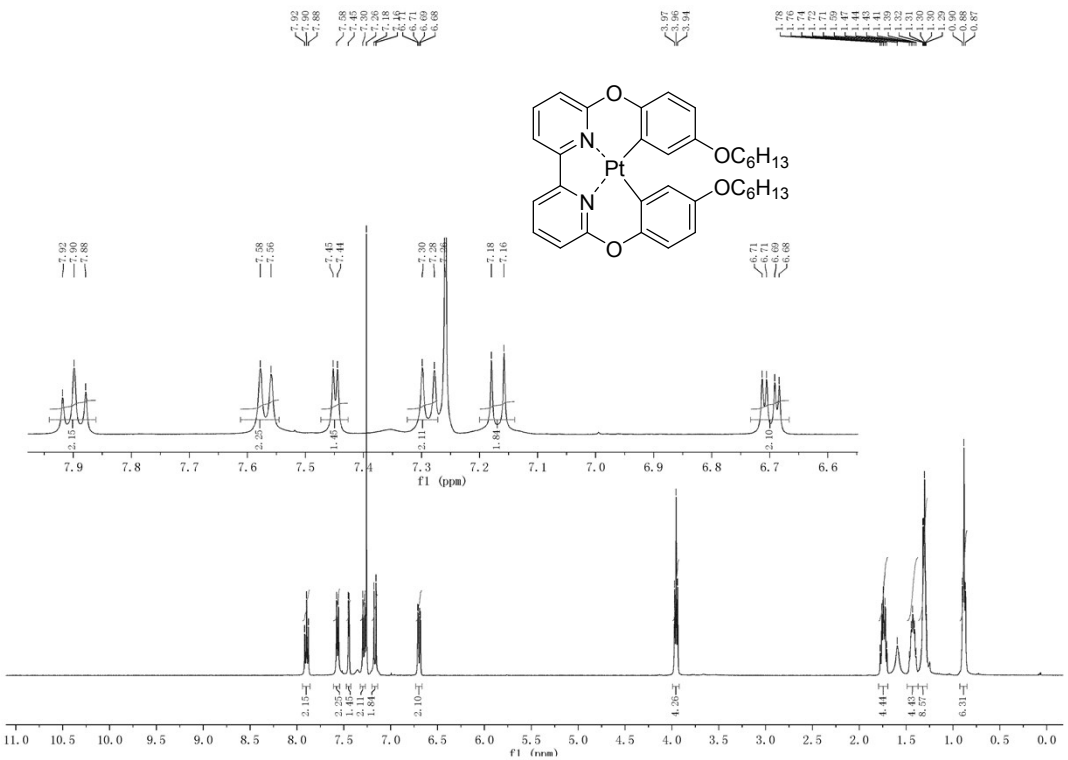

^{1}H NMR plot of **Pt-L^{12}**.

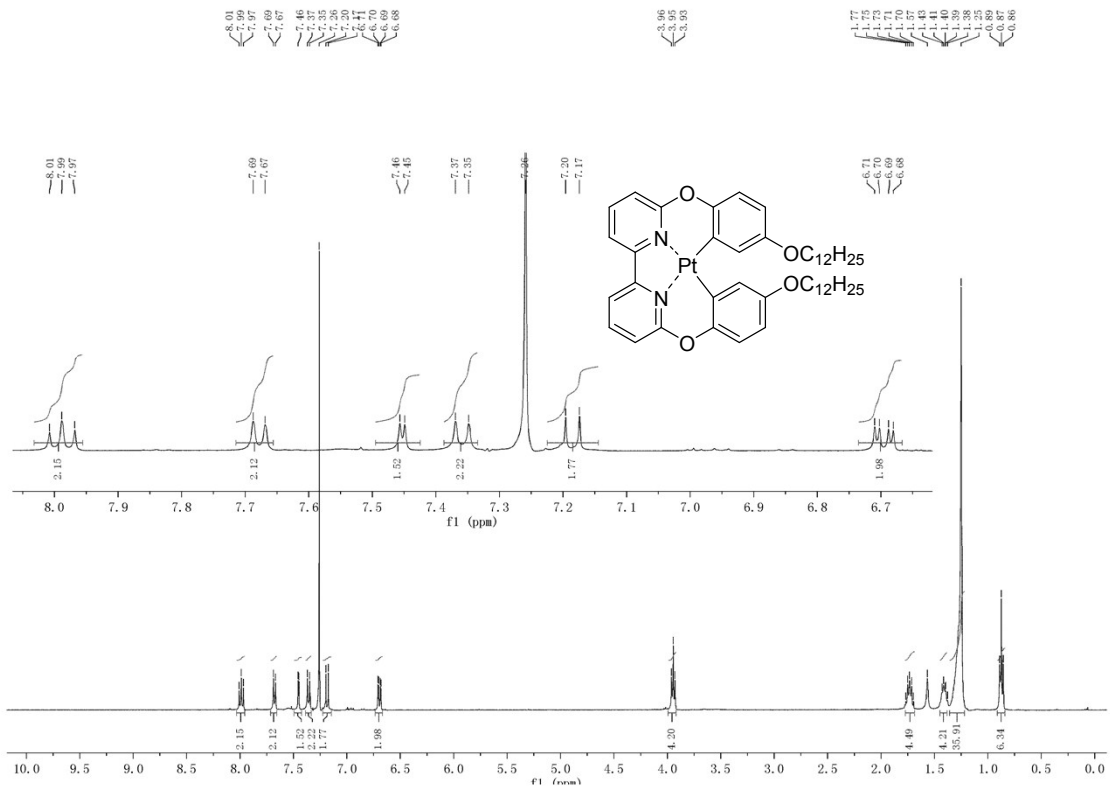

^{1}H NMR plot of **Pt-L^{16}**.

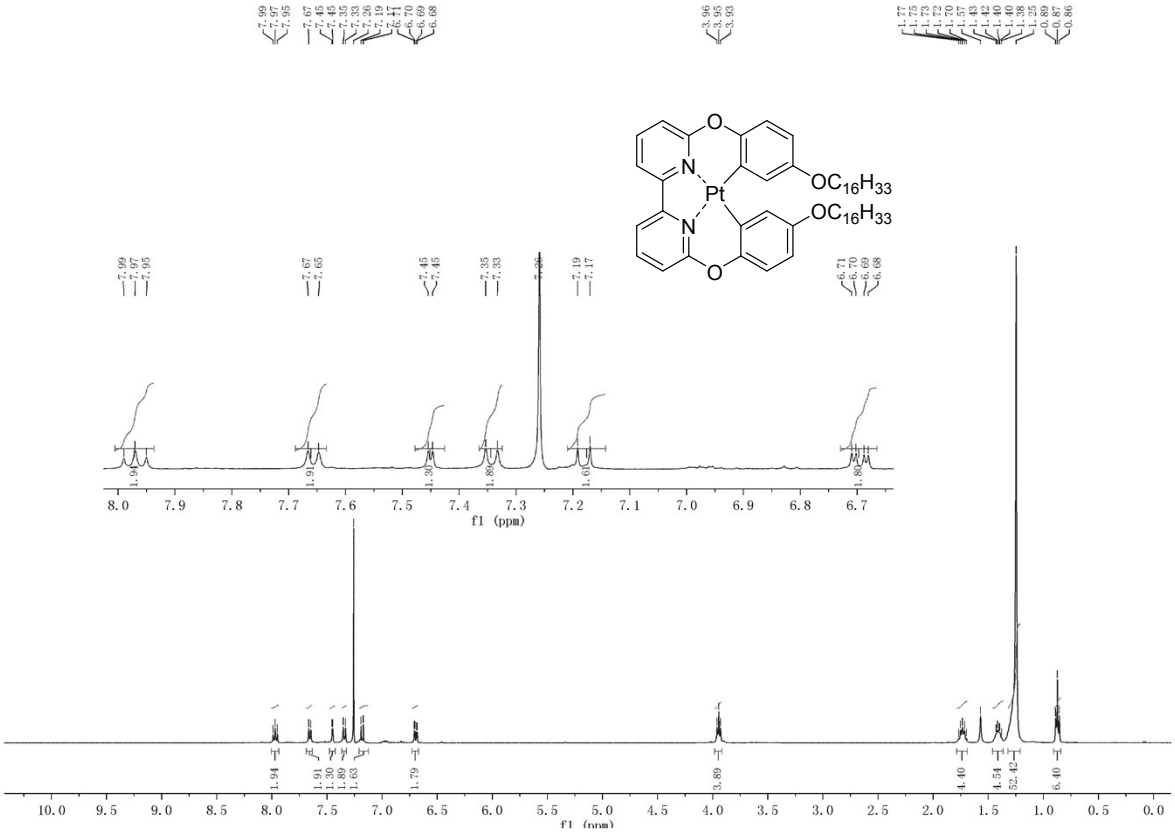

^{13}C NMR plot of **Pt-L^{6}**.

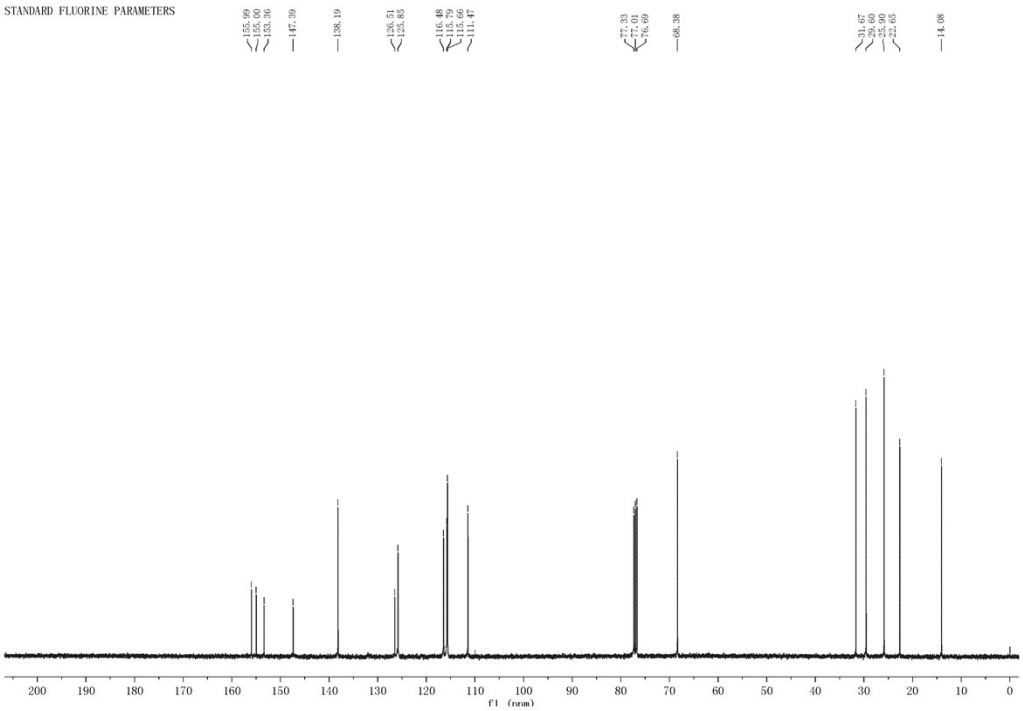

^{13}C NMR plot of **Pt-L^{12}**.

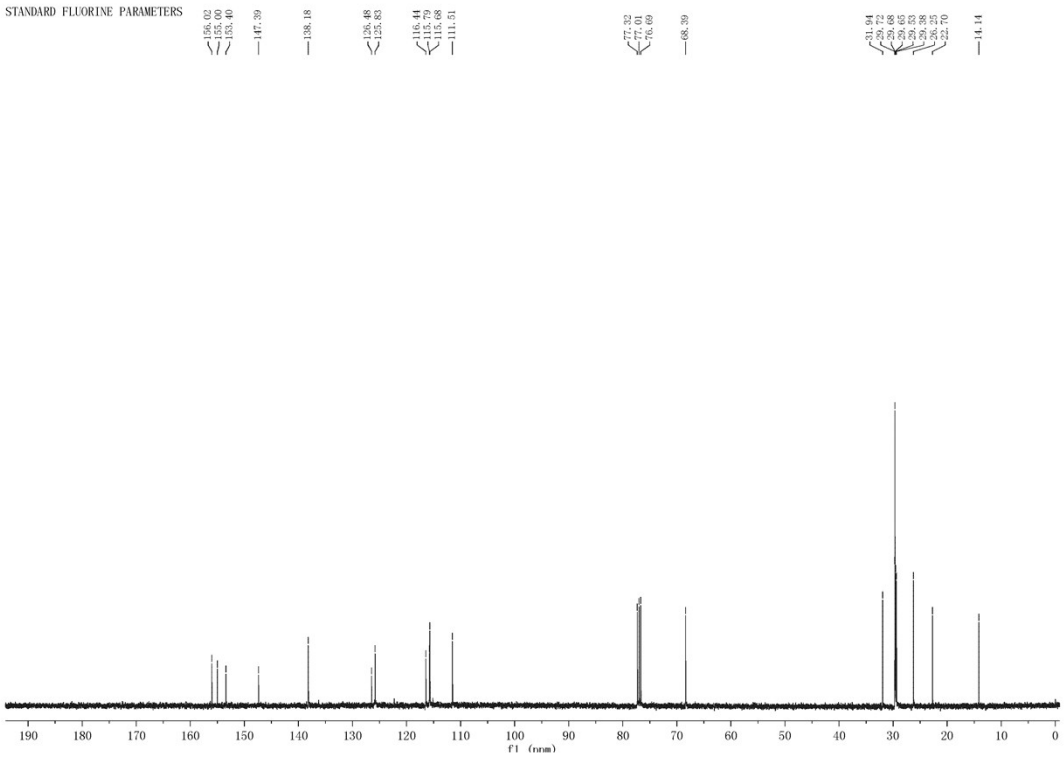

^{13}C NMR plot of **Pt-L^{16}**.

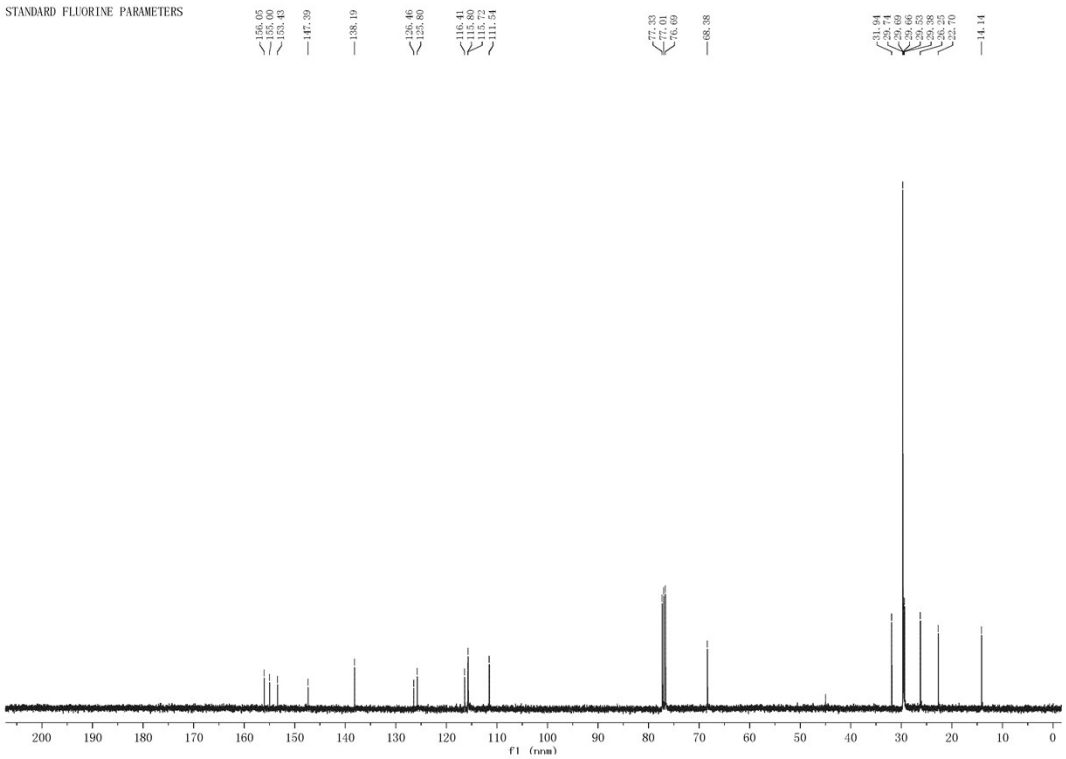

MS plot of **Pt-L^{6}**.

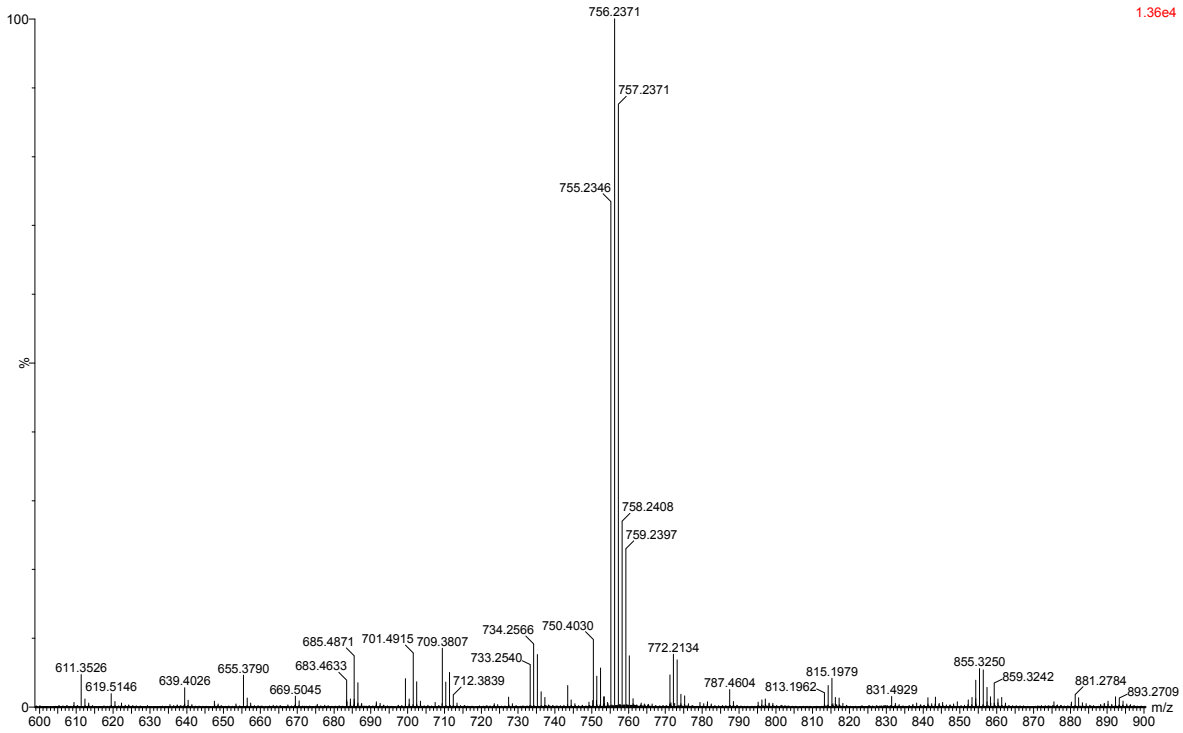

MS plot of **Pt-L^{12}**.

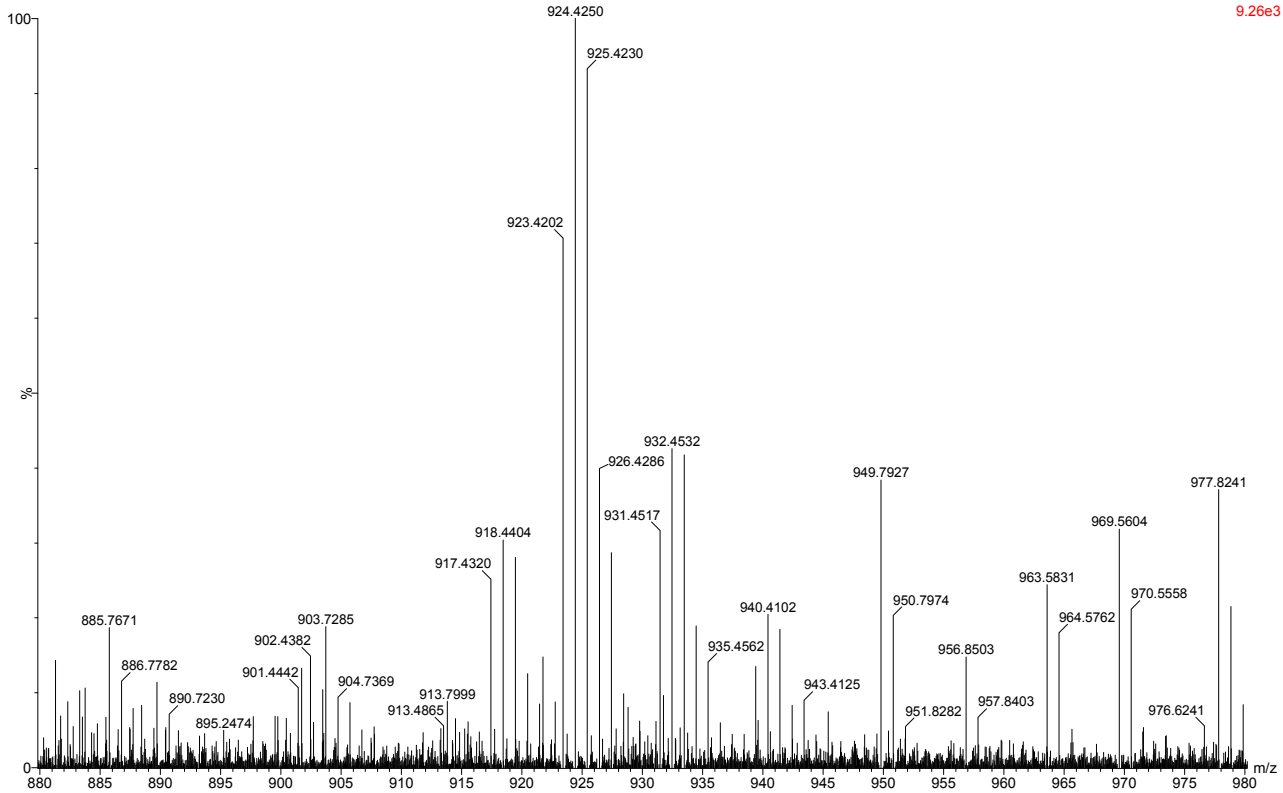

MS plot of **Pt-L**^{16}.